Cellulose (2020) 27:455–467
https://doi.org/10.1007/s10570-019-02804-3

ORIGINAL RESEARCH

Construction of ion-imprinted nanofiber chitosan films using low-temperature thermal phase separation for selective and efficiency adsorption of Gd(III)

Xudong Zheng · Tingting Bian · Yi Zhang · Yuzhe Zhang · Zhongyu Li

Received: 27 July 2019 / Accepted: 18 October 2019 / Published online: 1 November 2019
© Springer Nature B.V. 2019

Abstract Rare earth elements are a treasure trove of new materials in the twenty-first century, however, the similar radii of the lanthanide metals make it difficult for the ionic rare earth elements to be selectively separated. Ion-imprinted technology can help to selectively separate rare earth elements, nevertheless, most materials used for ion-imprinted are expensive. Chitosan has a wide range of sources, low cost, and a large quantity of amino and hydroxyl groups, which is advantageous for adsorbing heavy metals. Most scholars have made chitosan into a shape such as microspheres, which does not exert the great value of chitosan and is difficult to recycle, which greatly affects the adsorption rate. There are few studies on increasing the specific surface area of chitosan, so there is still much room for improvement in the adsorption capacity of chitosan. In order to improve the performance of chitosan-based materials, this research reports the preparation of imprinted nanofiber chitosan films (INFCF) by ion-imprinted technique and low-temperature thermal phase separation. These methods not only make the material have a high BET surface area, but also enable the material to have selective adsorption capacity. The BET surface area of the film is 203.6 m^2 g^{-1}. The maximum adsorption capacity of INFCF for Gd(III) was 71.00 mg g^{-1} at pH 7.0. The adsorption mechanism is summarized as a single layer of chemical adsorption. The excellent selectivity and repeatability of INFCF make it a high-quality material for the selective recovery of rare earth ions in industrial production.

Electronic supplementary material The online version of this article (https://doi.org/10.1007/s10570-019-02804-3) contains supplementary material, which is available to authorized users.

X. Zheng · T. Bian · Y. Zhang · Y. Zhang · Z. Li (✉)
School of Environmental and Safety Engineering, Changzhou University, 417 Mingxing Building, Science and Education City, Wujin District, Changzhou 213164, Jiangsu, People's Republic of China
e-mail: zhongyuli@mail.tsinghua.edu.cn

Z. Li
Jiangsu Key Laboratory of Advanced Catalytic Materials and Technology, School of Petrochemical Engineering, Changzhou University, Changzhou 213164, People's Republic of China

Z. Li
Advanced Catalysis and Green Manufacturing Collaborative Innovation Center, Changzhou University, Changzhou 213164, People's Republic of China

Graphic abstract

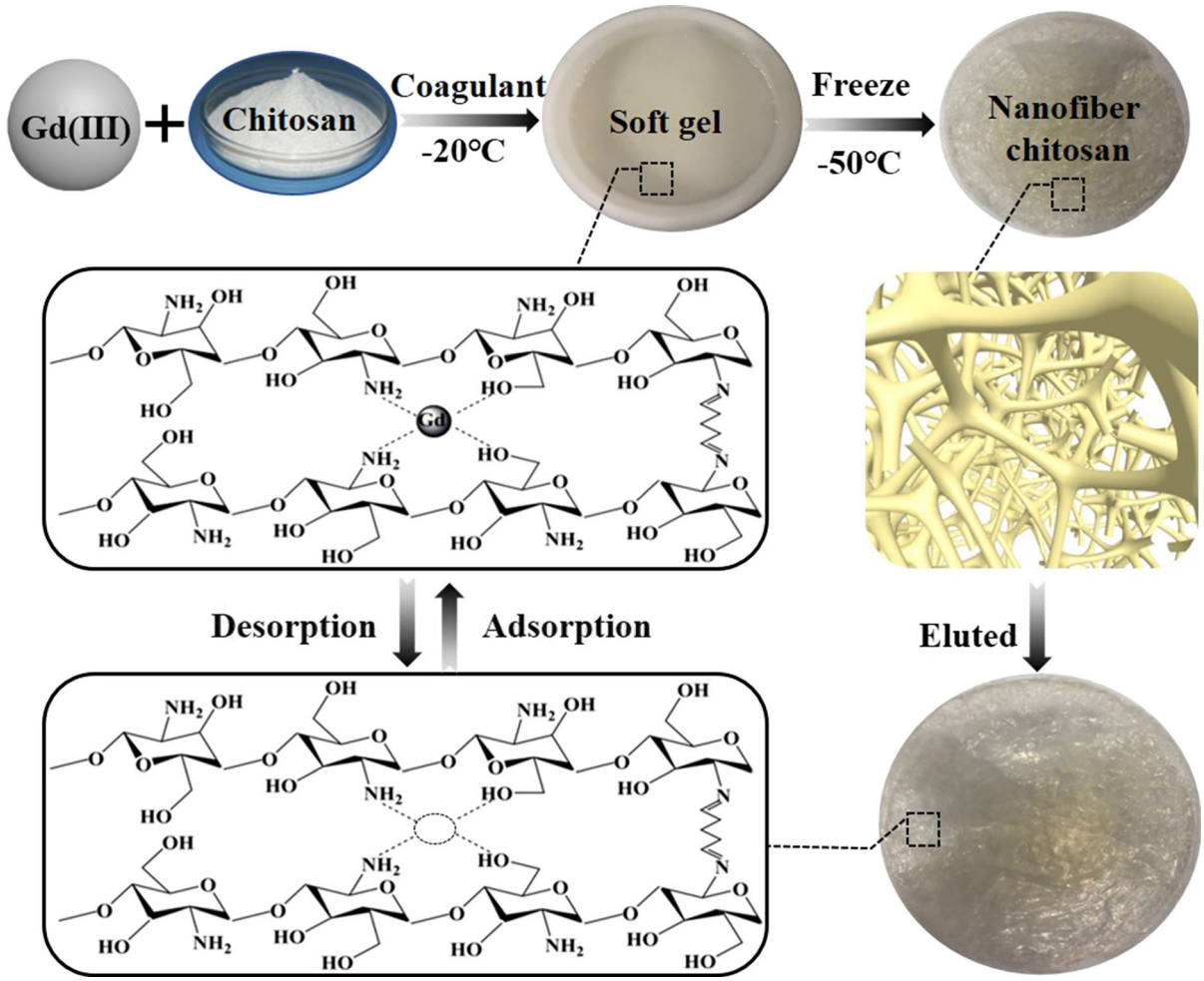

Keywords Ion-imprinting · Nanofiber chitosan films · Gd(III) · High specific surface area · Selective adsorption

Introduction

The rapid development of the economy and society has led to a sharp increase in demand for various commodities, and the use of special materials has become more widespread. Rare earth elements have the advantages of para-magnetism, low melting point, good plasticity, and high hardness are widely used in many fields such as new materials, military, electronic chips and chemicals (Zheng et al. 2016). Among them, gadolinium (Gd) is the element with the largest number of unpaired electrons. These physical and chemical properties make Gd a candidate for cutting-edge technology (Raebiger and Bolskar 2008). An important property of Gd is that there is one electron in each orbit in seven orbits, which is the largest number of unpaired electrons in the rare earth element. Depending on the magnetic moment of this unpaired electron, it is expected that this property can be effectively utilized in many fields such as medical, industrial and nuclear energy. However, increased demand for advanced products has led to a rapid increase in waste, especially Gd-containing wastewater. Incomplete treatment of Gd in water can have an irreversible negative impact on the environment and human health. Rare earth elements are difficult to be

separated due to similar ionic radii (Jha et al. 2016). Existing separation techniques [stepwise method (Habashi 2013; Martinez et al. 2013), liquid–liquid extraction method (El-Nadi 2017), membrane separation method (Tavlarides et al. 1987) and solid–liquid extraction method (Sun et al. 2008)] have certain effects in removing heavy metals from water. However, it is difficult to selectively separate a single heavy metal.

Ion-imprinted technique (IIT) is a good method for separating specific heavy metal ions from water. Depending on the ionic radius, IIT imprints a specific ion in a high molecular polymer to form a specific cavity after elution (Fu et al. 2015). IIT is widely used in the field of ion separation (Suquila et al. 2018; Wei et al. 2018b). Ide's team synthesized a monoamide-based adsorbent for selective adsorption of lanthanides (Nd(III)) based on ion imprinting and studied its adsorption characteristics. Density functional theory (DFT) calculation of a model system revealed that the ion-imprint effect and inhibition effect is the cause of large adsorption amount (Ide et al. 2016). Zhu's team made a two-dimensional surface imprinted polymer using montmorillonite to extract Pb(II) from slag (Zhu et al. 2018). Adsorption experiments confirmed the excellent selective adsorption properties of the material. Hao's team studied the selective adsorption of U(VI) from seawater, and their imprinted graphite carbonized composites showed excellent adsorption capacity and extraction selectivity for U(VI) (Hao et al. 2018). Although the above studies successfully solved the problem of selective adsorption, the adsorption capacity was not greatly improved. The difficulty in obtaining raw materials and the high cost are also great problems. The low adsorption capacity is mainly due to the small number of imprinting sites available for the material to provide an adsorption reaction. Therefore, we are committed to finding a low cost and highly efficient adsorbent.

Biomaterials are believed to have a large number of reactive functional groups. Among biomaterials, chitosan is one of the most excellent materials for adsorbing heavy metals because it contains a large amount of amino and hydroxyl groups (Liu et al. 2012). Chitosan is inexpensive, readily available, and is a green, non-polluting material. These advantages have led to the development of chitosan in many fields such as biochemistry, medicine and environmental protection (Rinaudo 2006). The combination of chitosan and IIT will greatly assist in the adsorption of rare earth elements (Baroni et al. 2008; Ngah et al. 2011; Shafaei et al. 2007). However, chitosan has some disadvantages, it is only soluble in weak acid, easy to agglomerate and low in specific surface area.

In order to overcome the problem that chitosan will dissolve in a weak acid solution; it is a feasible method to prepare chitosan into a stable form in advance. Some studies have made chitosan a blocky structure of hydrogels, but the use of chitosan as a bulk material reduces the active site of chitosan (Liu and Bai 2006; Yu et al. 2017). The pure aqueous solution of chitosan is difficult to have a large specific surface area and porous structure. The preparation of hollow fiber membranes by electrospinning and low temperature induced phase separation seems to be a good solution (Kim et al. 2016). However, electrospinning nanofiber production that the inorganic material having a larger brittleness (Kim et al. 2005).

Low-temperature thermal phase separation is more likely to produce porous nanofiber membranes than liquid–solid phase separation. It is a technique in which a polymer is dissolved in a mixed solvent to form a homogeneous solution in a film forming mixture at a temperature lower than the melting point of the polymer. It is then cooled to achieve phase separation. As long as the appropriate process conditions are controlled, the system can form a two-phase structure in which the polymer is the continuous phase and the solvent is the dispersed phase after the phase separation. So controlling the freezing point of the solvent is extremely important. It is well known that the addition of ethanol to a solvent can lower the freezing point of the solvent, and the low-temperature thermal phase separation can be initiated during the freeze-drying process to form a nanofiber porous structure. By these methods, chitosan has a high specific surface area, a nanofiber structure, and a selective adsorption capacity, so that the material can have a broader prospect in industrial applications (Erdeng et al. 2018; Wei et al. 2018a, 2019).

In this work, we prepared a chitosan film with nanofibers by using ion-imprinted technology and using ethanol to reduce the freezing point of the solvent to complete the low-temperature thermal phase separation technique. The purpose of efficiently and selectively adsorbing and separating Gd(III) ions from aqueous solution is achieved. We characterized the material by scanning electron microscope (SEM),

Fourier transform infrared (FTIR), N_2 adsorption–desorption, X-ray photoelectron spectroscopy (XPS) and thermogravimetric (TG). The adsorption and selection properties of Gd(III) on materials were investigated by a series of experiments on static and dynamic adsorption and simulation of actual samples.

Experimental

Materials

The reagents used in the experiment were chitosan, cerium nitrate hexahydrate, glacial acetic acid, absolute ethanol, and glutaraldehyde. The degree of deacetylation of chitosan is 95–100%. The concentration of glutaraldehyde is 50%.

Preparation of materials

The imprinted nanofiber chitosan film (INFCF) was prepared in the following procedure. The chitosan with a concentration of 2% W/V was dissolved in acetic acid solution (2% V/V, anhydrous ethanol in the solvent: water = 3:7), and 0.5 g of gadolinium nitrate hexahydrate was added, and the mixture was uniformly mixed at room temperature. The bubbles in the solution were removed under ultrasound. The solution was poured into a Teflon tray and allowed to stand at 253 K for 10 h until the solution became a clear soft gel. Subsequently, a coagulant (1 M NaOH) was added and the coagulant was pre-frozen at 273 K. The soft gel was allowed to stand at 273 K for 6 h to become a milky white soft gel. Pour 3 M glutaraldehyde into the dish to crosslink. Distilled water was then poured into the petri dish and distilled water was changed every 8 h until it became neutral. After freezing at 253 K for 2 h, it was freeze-dried at 223 K for 24 h. The Gd(III) was eluted using a mixed solution of glacial acetic acid: DDW = 1:9.

The experimental procedure for the non-imprinted nanofiber chitosan film (NNFCF) was identical to that of the INFCF without Gd(III).

Adsorption experiment

We performed pH, kinetic, isotherm, competitive adsorption, thermodynamics, and repeatability experiments on INFCF and NNFCF. Specific experimental steps are placed in the supplementary material. All experimental results were obtained by ICP detection.

Characterization analysis means

A chain of characterizations was performed on successfully prepared NFCF. The surface structure of NFCF was observed to form a nanofiber shape by photographing SEM. The functional groups present in the molecule of NFCF was observed by FTIR. The surface area of NFCF was analyzed by N_2 adsorption–desorption method. The Zeta point was used to analyze the surface charge of NFCF. Thermal stability was observed by TG. The change in elemental content of C, N, O, and Gd(III) was analyzed by XPS. The above six characterizations were used to verify that the NFCF material has a good nanofiber structure and excellent adsorption properties.

Results and discussion

Analysis of characterization results

SEM

The surface topography of the film can be observed by SEM (Fig. 1). (a) is the surface topography, and it can be seen that a large number of pore structures form a network and are joined together. The (a) picture is enlarged to obtain (b) picture, and the (b) picture clearly shows that the inside of the film is also a nanofiber structure. The (c) picture shows the SEM image of the cut surface. It can also be seen from the cut surface that the fiber structure inside the film is very obvious. This demonstrates that low temperature thermally induced phase separation techniques have successfully formed nanofiber structures. The uneven distribution of the nanofiber structure increases the specific surface area of the film, and the active adsorption sites exposed to the chitosan surface also increase correspondingly, which contributes to the improvement of the material adsorption capacity.

FTIR

The FTIR spectra of NNFCF and INFCF are shown in Fig. 2. NNFCF and INFCF have similar peaks in the range of 4000–500 cm^{-1}. The formation of a polymer

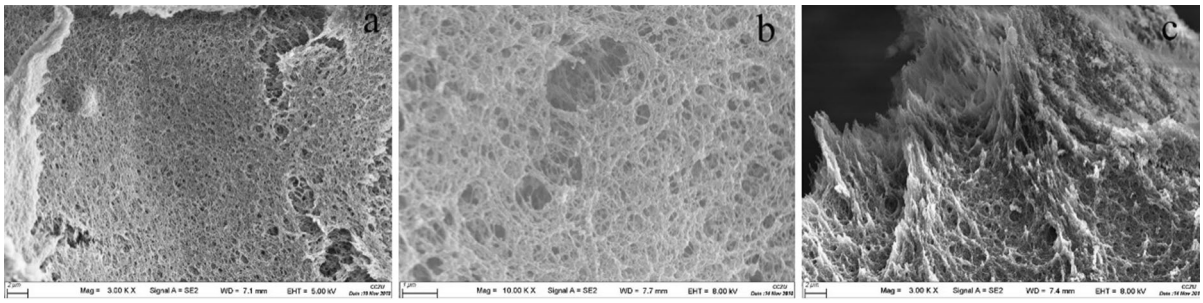

Fig. 1 SEM image of INFCF

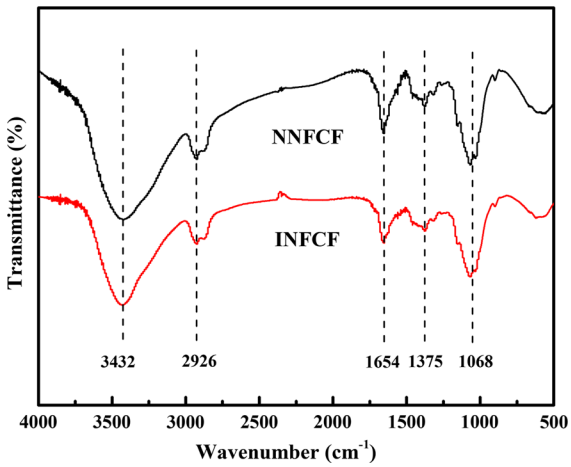

Fig. 2 The FTIR of NNFCF and INFCF

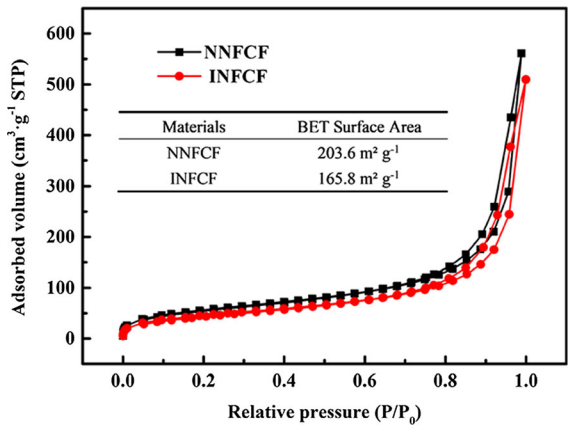

Fig. 3 N_2 adsorption–desorption isotherm plot of films

by an amide group by hydrogen bonding causes a stretching vibration of N–H to cause a peak at 3432 cm^{-1}. The absorption peak at 2926 cm^{-1} is caused by asymmetric stretching of CH_2 and stretching vibration of C–H. The bending vibration of N–H caused the amide II band at 1654 cm^{-1}. Due to the resonance effect, the stretching vibration of C=O causes an absorption peak at 1375 cm^{-1}. The absorption peak at 1068 cm^{-1} is caused by the stretching vibration of the symmetric C–O–C. The intensity of the absorption peak of INFCF at 1068 and 3432 cm^{-1} was lower than that of NNFCF, indicating that the imprinted ions occupied part of the $–NH_2$ and –OH groups during the imprinting process.

N_2 adsorption–desorption (BET test method)

The physical adsorption mechanism of the material was investigated by N_2 adsorption–desorption analysis method. The isotherm is shown in Fig. 3 belongs to the type IV adsorption isotherm. When the relative pressure is in the low-pressure region between 0.0 and 0.05 P/P_0, the curve is convex upward, and single layer adsorption is first formed, and the multilayer adsorption is started when the saturated adsorption amount of the monolayer is reached. The relative pressure of the multilayer adsorption is between 0.05 and 0.75 P/P_0. As the gas pressure increases, the pores of the gas agglomerate become larger and larger, causing hysteresis, and the desorption isotherm formed a hysteresis loop above the adsorption isotherm. The hysteresis loop belongs to the H3 type, and when the relative pressure is close to the saturated vapor pressure, the balance is not reached, and the surface material is a slit-like hole formed by the polymer sheet-like particles. The BET surface area of the material is 203.6 $m^2\ g^{-1}$, and the large BET surface area is very helpful for the adsorption reaction. From the specific surface area data in Fig. 3, it can be seen that the specific surface area of INFCF is 37.8 $m^2\ g^{-1}$ less than that of NNFCF. There are two main reasons for

this phenomenon. The first is that the nanofiber structure constructed by the phase separation technique achieved by freeze drying is random. Therefore, the specific surface area of the nanofiber structure formed in different molds is also slightly different. Then the addition, cross-linking and elution of metal ions have a small effect on the structure of the material, resulting in a slightly smaller specific surface area of INFCF than NNFCF.

Zeta potential

The zeta test was measured at diverse pH values and the results are shown in Fig. 4. The zeta potential is a characteristic of the amount of charge on the surface of the particle, which is related to the stability of the particle system. The pH affects the presence of cations in the solution and the surface charge of the adsorbent. In order to avoid precipitation of rare earth ionic hydroxide under alkaline conditions, adsorption properties in the pH range of 2.0–7.0 were investigated. The Zeta potential is the potential difference between the continuous phase and the fluid stabilizing layer attached to the dispersed particles. It can be measured directly by electrokinetic phenomena. This is also related to the protonation of acidic conditions to protonation of the surface to increase the positive charge. The isoelectric point occurred at pH 6.0 and 6.5, respectively. Both materials have an electrostatic negative charge on the surface at pH 7.0, which is the most favorable condition for adsorbing cationic heavy metals.

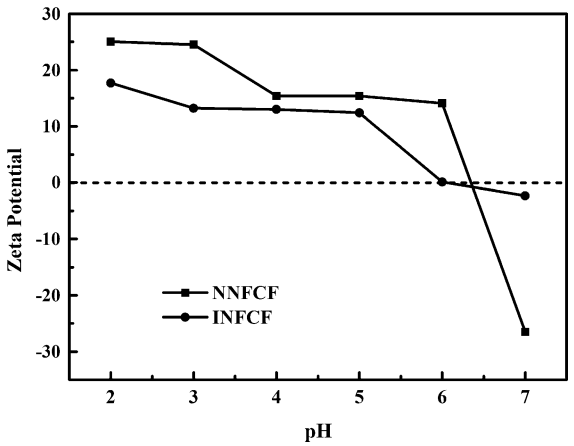

Fig. 4 Zeta potential of NNFCF and INFCF

TG analysis

In order to study the thermal stability of the material, we performed a TG test to analyze the relationship between mass and temperature change of the material at programmed temperature. We not only analyzed the ratio of the weight of the sample at the current temperature to the initial weight, but also analyzed the TG calculus curve (DTG). That is, the curve obtained by differentiating each time coordinate on the TG curve, it is a means of characterizing the change in the rate of weight change with temperature. The TG analysis of NNFCF and INFCF can be clearly seen from Fig. 5. It is well known that chitosan can withstand heat at around 100 °C. The weight loss in the figure at 100 °C is the loss of crystal water in the film. The extrapolation starting point of the TG curve of the self-crosslinking chitosan (the starting point of the weight loss process) was at 250 °C, and the weight loss process was terminated at around 500 °C. The weight lost during this time is chitosan. Compared with ordinary chitosan, the thermal stability of the material has been improved. The INFCF retained a total of 35% after a high temperature of 800 °C.

XPS

We use X-rays to irradiate the sample to stimulate the emission of the inner or valence electrons of the atom or molecule. The energy of the photoelectrons can be measured to obtain the composition of the analyte. The changes in the elements detected by XPS are shown in Fig. 6. A large number of hydroxyl groups and amino groups contained in chitosan are not lost by imprinting, and the amount of loss is negligible. Therefore, the original adsorption capacity of chitosan is retained simultaneously with imprinting. Due to the metal ions remaining inside the material, only 0.07% of the metal ions remained after the elution experiment. The peak of C1*s* is red-shifted, indicating the formation of a sorbent–metal complex and reducing the electron density of C–O, C=N, and C=O. The collective energy shift of N1*s* indicates that after adsorption of Gd(III), in addition to –COOH, lone pairs of electrons in the $–NH_2$ group also help in $–NH_2$ and Gd(III). After various characterization tests, the adsorption experiments were carried out on the materials, and the separation and recognition rules and adsorption mechanism of Gd(III) were further discussed.

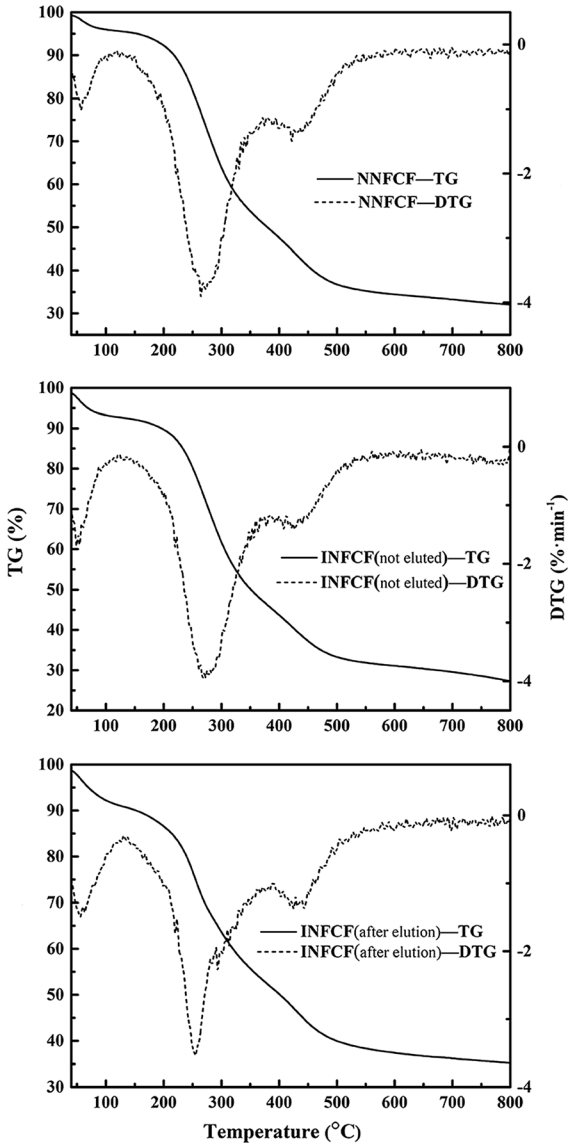

Fig. 5 Thermogravimetry of INFCF and NNFCF

Adsorption experiment analysis

pH experiment

The pH has a large effect on the metal ion adsorption of the material. The film exhibits different surface properties at different pH conditions, which results in a difference in adsorption capacity. In this work, six different pH values were chosen to study. We let NNFCF and INFCF react under the same conditions. Since Gd(III) readily precipitates under alkaline conditions, the pH range of this experiment is 2.0–7.0. The experimental results are shown in Fig. 7. It is apparent from the figure that the overall tendency of the number of adsorptions increases as the pH value increases. Under acidic conditions, H^+ is present in a large amount in the solution, and is easily combined with a lone pair of electrons of $–NH_2$ through a coordination bond to form $–NH_3^+$. When the $–NH_2$ of CS is protonated to $–NH_3^+$, the chelation ability with metal ions is reduced. At the same time, the surface of the adsorbent generally exhibits a positive charge, which is not conducive to the adsorption of metal cations (Pan et al. 2016). The amino group on the surface of chitosan is prone to protonation under acidic conditions, and the zeta potential map also shows that when the pH of the solution is < 6.0, the surface of the film is positively charged. This phenomenon reflects from the side that the amino group under acidic conditions is protonated. Adsorption mainly depends on the binding of metal ions to the amino group on chitosan, so the protonation of amino groups under acidic conditions largely affects the adsorption capacity of the film. In summary, we chose pH 7.0 as the best condition for subsequent experiments.

Adsorption kinetics experiment

The adsorption kinetics experiment is a method to study when the material reaches the adsorption equilibrium. We set different adsorption times and tested the remaining concentration of Gd(III) in the solution. The data for adsorption kinetics were fitted using a pseudo-first-order kinetic model (PFOKM) and a pseudo-second-order kinetic model (PSOKM).

Figure 8 shows the kinetic curves of NNFCF and INFCF, both of which show a rapid increase between 0 and 100 min, with the subsequent increase in gradual tendency. In the entire adsorption kinetics curve, the adsorption capacity rises rapidly within 30 min, representing a fast mass transfer efficiency. Adsorption stops at 300 min to reach equilibrium, but there was a slow upward trend after 300 min. The reason for this phenomenon may be that the surface of the film reaches the saturation of adsorption, and it takes a certain time for the metal ions to reach the inside of the film through the gap to achieve a true balance. The formation of the imprinting site improves the adsorption performance of the film, resulting in a slightly larger adsorption amount than the non-imprinted film.

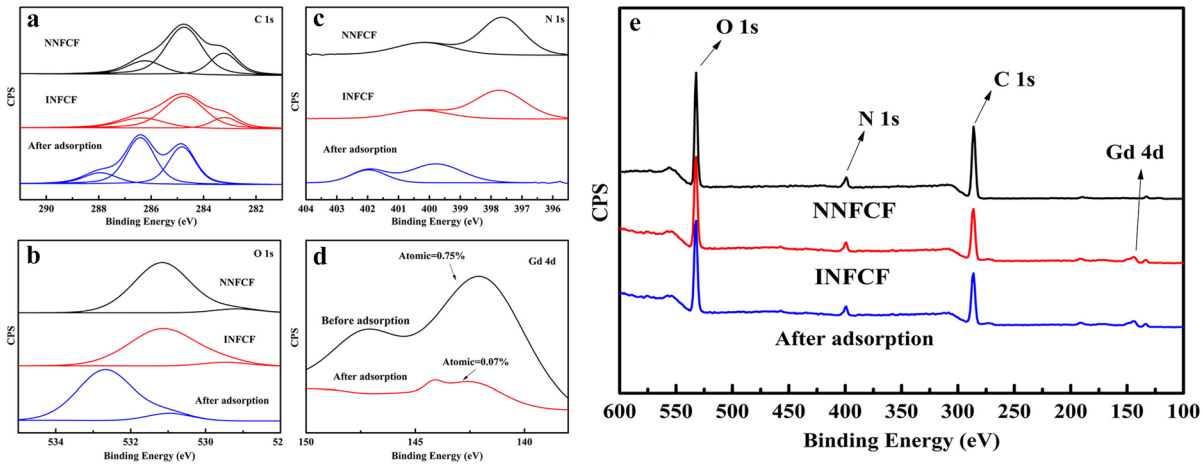

Fig. 6 XPS energy spectrum of NNFCF and INFCF

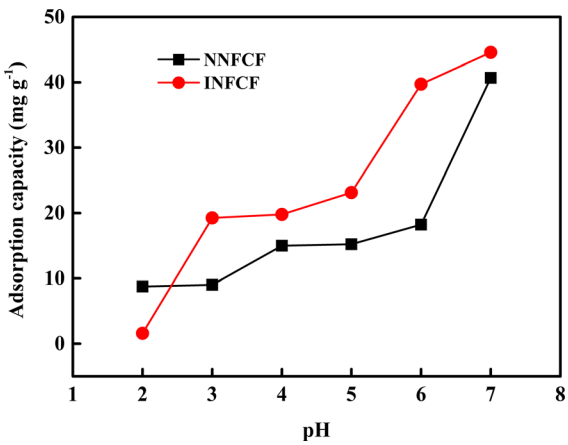

Fig. 7 Effect of pH on the adsorption of Gd(III) on INFCF and NNFCF

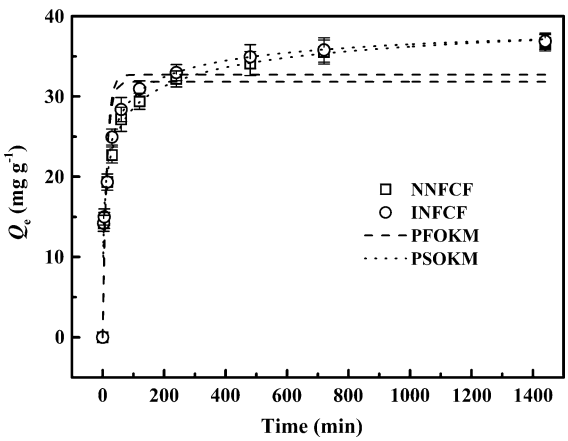

Fig. 8 Kinetic data and model of Gd(III) adsorption on NNFCF and INFCF

The 3D imprinting cavity that matches the target ions helps the material capture target ions quickly and efficiently. However, active groups on the surface of chitosan have been shown to have excellent adsorption capacity, so NNFCF and INFCF are highly adsorbed. The kinetic parameters of the film and the corresponding correlation coefficient (R^2) are shown in Table 1. It can be clearly observed from Table 1 that the correlation coefficient of the film PSKOM is closer to 1. The R^2 of NNFCF and INFCF are 0.994 and 0.990, respectively. Meanwhile, the adsorption rate of the adsorption process is proportional to the flatness of the quantity of imprinting site in the film, and the adsorption mechanism is a chemical reaction process.

Adsorption isotherms

The adsorption isotherm can accurately measure the maximum adsorption capacity of the film for Gd(III). NNFCF and INFCF were reacted in different concentrations of the solution and fit the data obtained.

The fit of adsorption isotherm in Fig. 9, it can be clearly seen that the fitting result is closer to the Langmuir isotherm. This also indicates that the dominant type of adsorption is a single layer of chemical adsorption and the possibility that the adsorbate occupies all adsorption sites is the same. The probability that a Gd(III) is adsorbed at one site is independent of other factors. The main way for INFCF to adsorb ions is the selective adsorption of ions by the imprinted site, while the NNFCF adsorbs ions mainly relying on the active groups on the chitosan surface.

Table 1 Kinetic constants for the PFOKM and PSOKM

Materials	$Q_{e,exp}$ (mg g^{-1})	PFOKM			PSOKM				
		$Q_{e,c}$ (mg g^{-1})	k_1 (min^{-1})	R^2	$Q_{e,c}$ (mg g^{-1})	$K_2 \times 10^{-2}$ (g mg^{-1} min^{-1})	h (mg g^{-1} min^{-1})	$t_{1/2}$ (min)	R^2
NNFCF	36.70	31.83	0.08	0.839	43.07	0.63	11.77	3.66	0.994
INFCF	36.87	32.72	0.08	0.870	40.54	0.67	11.05	3.67	0.990

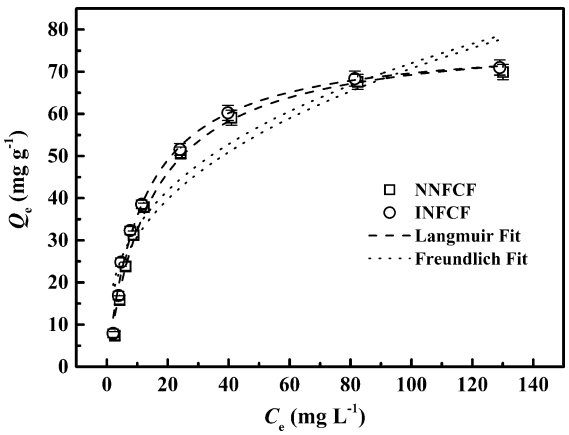

Fig. 9 Isotherm model fitting of NNFCF and INFCF adsorbing Gd(III)

The saturated adsorption capacities of NNFCF and INFCF were 69.93 and 71.00 mg g^{-1}. The adsorption and separation performance of the imprinted film is stronger than that of the non-imprinted film, which indicates that the formation of the imprinting site not only enables the membrane to have a specific selective adsorption capacity but also improve the efficiency in the adsorption process, resulting in excellent adsorption performance. The R_L of NNFCF and INFCF were found to be 0.17 and 0.14, respectively, from the adsorption isotherm fitting data (Table 2). The R_L value of INFCF is less than NNFCF, which shows that INFCF is a more favorable adsorbent and confirms the superiority of ion-imprinted technology.

Adsorption thermodynamics

Further, in order to explore the effects of thermal motion properties on adsorption, we performed a thermodynamic analysis of the film. The same adsorption experiments were performed at 298.15, 308.15, and 318.15 K, respectively.

The results of the thermodynamic data are shown in Fig. 10, and it can be visually seen that the adsorption capacity increases correspondingly with an increase in temperature. The reason for this phenomenon is that the increase in temperature exacerbates the diffusion movement between molecules. The thermodynamic data is shown in Table 3, where $\Delta H > 0$ indicates that the adsorption reaction is an endothermic reaction, and the increase in heat contributes to the expansion of the adsorption capacity. $\Delta G < 0$ indicates that the reaction is spontaneous and does not require artificial addition of a catalyst. The analysis of thermodynamic properties helps us to further analyze the adsorption mechanism.

Adsorption selectivity study

The similar physical and chemical properties between rare earth elements are the main factors limiting the separation of high purity individual ions. According to our previous research, the surface sites provided by the surface imprinted material allow specific adsorption of target ions. In order to verify the unique adsorption

Table 2 Adsorption equilibrium constants for Langmuir and Freundlich isotherm equations

Sorbents	Langmuir isotherm equation				Freundlich isotherm equation		
	R^2	K_L (L mg^{-1})	Q_m (mg g^{-1})	R_L	R^2	K_F (mg g^{-1})	$1/n$
NNFCF	0.990	0.07	69.93	0.17	0.888	13.54	0.36
INFCF	0.992	0.09	71.00	0.14	0.899	15.17	0.34

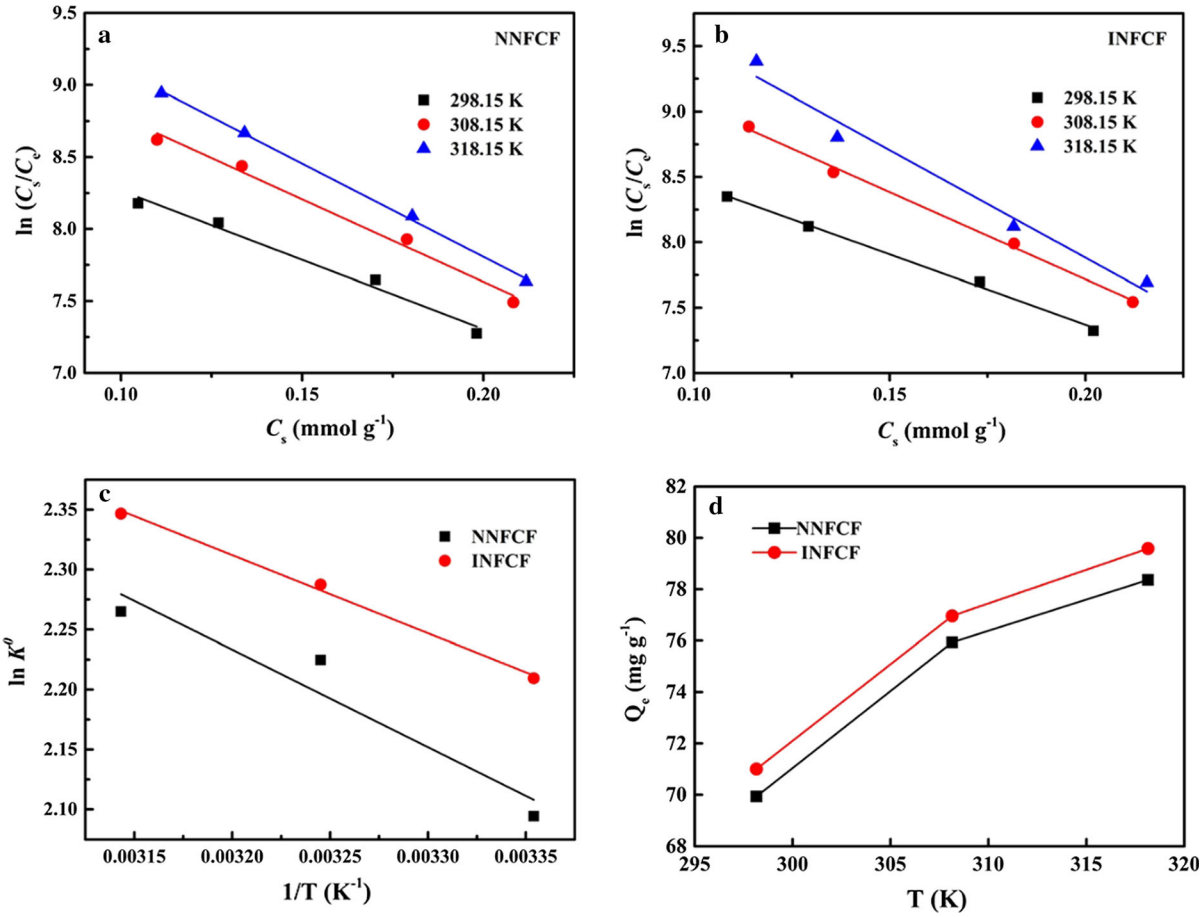

Fig. 10 Thermodynamic properties of Gd(III) at NNFCF and INFCF at 298.15, 308.15, and 318.15 K

Table 3 Thermodynamic parameters for Gd(III) adsorption

Materials	ΔH (kJ mol^{-1})	ΔS (J mol^{-1})	T (K)	K°	ΔG (kJ mol^{-1})	R^2
NNFCF	6761.28	40.24	298.15	9.23	− 5.51	0.850
			308.15	9.93	− 5.88	
			318.15	10.40	− 6.19	
INFCF	5417.40	36.58	298.15	9.52	− 5.59	0.993
			308.15	10.39	− 6.00	
			318.15	11.17	− 6.38	

selectivity of the imprinted film, La(III), Nd(III), and Sm(III) were selected as interference ions to participate in the competition experiment. (For details, please refer to the supplementary materials).

The k' values of Gd(III)/La(III), Gd(III)/Nd(III), and Gd(III)/Sm(III) of INFCF are 58.97, 31.03 and 32.06 times of NNFCF, respectively. Obviously, the K_d value of the imprinted composite film is much higher than the K_d value of the non-imprinted film. The excellent selectivity of INFCF for Gd(III) can be observed from Fig. 11. The data in Table 4 shows that the adsorption performance of INFCF for Gd(III) is 50.71, 32.27 and 39.44 times of La(III), Nd(III), and Sm(III), respectively. Excellent selective adsorption capacity depends on the formation of specific imprinting sites that prevent INFCF from binding to other metal ions.

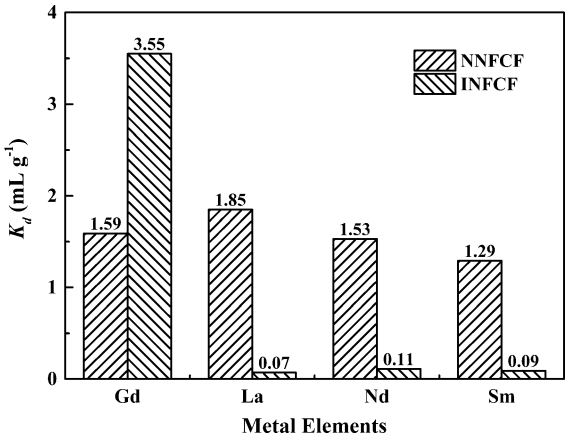

Fig. 11 K_d plot of INFCF competition experiment

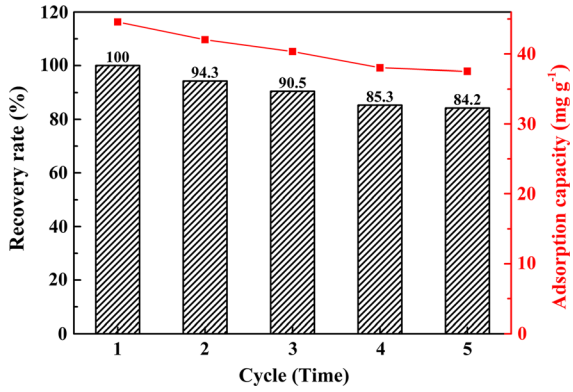

Fig. 12 Regeneration of INFCF

Regeneration experiment

The reusability of a film is an important indicator of its industrial value. The regeneration ability of INFCF was evaluated by 5 cycles of experiments. The remaining capacity of the adsorption capacity after the cycle is shown in Fig. 12, it is not difficult to see that the INFCF still maintains an adsorption capacity of 84.2% after 5 cycles. These losses are due to incomplete desorption or reduced active sites during cyclic elution. But INFCF still maintains excellent stability and reproducibility.

Compared

Adsorbent evaluation is considered by studying adsorption capacity, stability, and reusability. Compared with other scholars' materials (see Table 5), in the adsorption experiment of rare earth elements, INFCF has higher adsorption capacity than other modified bio-sorbents, and the adsorption effect under neutral conditions is the best. More advantageously, INFCF has excellent selective adsorption capacity. In general, INFCF not only has good selective adsorption properties, but also has high adsorption capacity, good stability and easy recycling.

Conclusion

Chitosan films with porous nanofibers were prepared by ion-imprinting technique and low-temperature thermal phase separation technique, and Gd(III) were selectively adsorbed and separated from the simulated sample. A series of characterization methods have proved that the film has excellent adsorption performance and stability. The adsorption performance of INFCF on Gd(III) was studied by a series of static and dynamic adsorption tests. The experimental results show that when pH 7.0, the maximum adsorption capacity of the membrane at 298.15 K is 71.00 mg g^{-1}. The adsorption kinetics and adsorption isotherms of INFCF conform to the PSOKM and Langmuir isotherms, respectively, revealing the adsorption mechanism of INFCF monolayer chemisorption. The wide range of chitosan sources, ease of preparation, and has a huge amount of active sites make our films stand out in the same type of

Table 4 K_d, k and k' values of La(III), Nd(III) and Sm(III) with respect to Gd(III)

Metal ions	NNFCF			INFCF			k'
	C_f (mg L^{-1})	K_d (mL g^{-1})	k	C_f (mg L^{-1})	K_d (mL g^{-1})	k	
Gd(III)	14.34	1.59		10.99	3.55		
La(III)	17.54	1.85	0.86	46.75	0.07	50.71	58.97
Nd(III)	19.75	1.53	1.04	45.01	0.11	32.27	31.03
Sm(III)	24.83	1.29	1.23	45.89	0.09	39.44	32.06

Table 5 Compared with other chitosan materials

Adsorbents	Ions	Q_m (mg g^{-1})	pH	References
INFCF	Gd(III)	71.00	7.0	This work
IIBFs	Nd(III)	17.50	4.0	Zheng et al. (2018)
Thiourea functionalized cellulose	Eu(III)	27.00	–	Negrea et al. (2018)
IMCFs	Gd(III)	25.37	7.0	Zheng et al. (2019b)
Diglycolamide polymer modified silica	Eu(III)	59.40	–	Liu et al. (2019)
DIMFs	Rb(I)	6.21	7.0	Zheng et al. (2019a)

adsorbent. The stability and reusability of INFCF also make it more promising for industrial applications.

Acknowledgments This work was financially supported by National Natural Science Foundation of China (Nos. 21876015, 21808018, 21822807), Applied Basic Research of Changzhou (No. CJ20180055), Natural Science Research of Jiangsu Higher Education Institutions of China (No. 18KJB610002), Science and Technology Support Program of Changzhou (No. CE20185015), and Postgraduate Research & Practice Innovation Program of Jiangsu Province (No. SJCX18_0958). The authors would like to thank Wang Liang from Shiyanjia Lab (www.shiyanjia.com) for the XPS analysis. Also, the author would like to thank the researchers at the Analytical Testing Center of Changzhou University for their assistance in SEM, FTIR, and BET analysis.

Compliance with ethical standards

Conflict of interest The authors declare no competing financial interest.

References

Baroni P, Vieira R, Meneghetti E, Da Silva M, Beppu M (2008) Evaluation of batch adsorption of chromium ions on natural and crosslinked chitosan membranes. J Hazard Mater 152(3):1155–1163

El-Nadi Y (2017) Solvent extraction and its applications on ore processing and recovery of metals: classical approach. Sep Purif Rev 46(3):195–215

Erdeng D, Jiaqi L, Siqi Z, Lu Z, Xinxin F (2018) Transformation of naproxen during the chlorination process: products identification and quantum chemistry validation. Chemosphere 211:1007–1017

Fu J, Chen L, Li J, Zhang Z (2015) Current status and challenges of ion imprinting. J Mater Chem A 3(26):13598–13627

Habashi F (2013) Extractive metallurgy of rare earths. Can Metall Q 52(3):224–233

Hao X, Chen R, Liu Q, Liu J, Zhang H, Yu J, Li Z, Wang J (2018) A novel U (vi)-imprinted graphitic carbon nitride composite for the selective and efficient removal of U (vi) from simulated seawater. Inorg Chem Front 5(9):2218–2226

Ide T, Suzuki A, Imada T (2016) Lanthanide selective adsorption by ion-imprinted polymer with chelidonic acid monoamide groups. Sep Sci Technol 51(18):2887–2895

Jha MK, Kumari A, Panda R, Kumar JR, Yoo K, Lee JY (2016) Review on hydrometallurgical recovery of rare earth metals. Hydrometallurgy 165:2–26

Kim GM, Lach R, Michler GH, Chang YW (2005) The mechanical deformation process of electrospun polymer nanocomposite fibers. Macromol Rapid Commun 26(9):728–733

Kim JF, Kim JH, Lee YM, Drioli E (2016) Thermally induced phase separation and electrospinning methods for emerging membrane applications: a review. AIChE J 62(2):461–490

Liu C, Bai R (2006) Adsorptive removal of copper ions with highly porous chitosan/cellulose acetate blend hollow fiber membranes. J Membr Sci 284(1–2):313–322

Liu L, Li C, Bao C, Jia Q, Xiao P, Liu X, Zhang Q (2012) Preparation and characterization of chitosan/graphene oxide composites for the adsorption of Au(III) and Pd (II). Talanta 93:350–357

Liu Z, Liu Y, Gong A (2019) Preparation of diglycolamide polymer modified silica and its application as adsorbent for rare earth ions. Des Monomers Polym 22(1):1–7

Martinez AM, Kjos O, Skybakmoen E, Solheim A, Haarberg GM (2013) Extraction of rare earth metals from Nd-based scrap by electrolysis from molten salts. ECS Trans 50(11):453–461

Negrea A, Gabor A, Davidescu CM, Ciopec M, Negrea P, Duteanu N, Barbulescu A (2018) Rare earth elements removal from water using natural polymers. Sci Rep-UK 8(1):316

Ngah WW, Teong L, Hanafiah M (2011) Adsorption of dyes and heavy metal ions by chitosan composites: a review. Carbohydr Polym 83(4):1446–1456

Pan JM, Zeng J, Cao Q, Gao HP, Gen YC, Peng YX, Dai XH, Yan YS (2016) Hierarchical macro and mesoporous foams synthesized by HIPEs template and interface grafted route for simultaneous removal of λ-cyhalothrin and copper ions. Chem Eng J 284:1361–1372

Raebiger JW, Bolskar RD (2008) Improved production and separation processes for gadolinium metallofullerenes. J Phys Chem C 112(17):6605–6612

Rinaudo M (2006) Chitin and chitosan: properties and applications. Prog Polym Sci 31(7):603–632

Shafaei A, Ashtiani FZ, Kaghazchi T (2007) Equilibrium studies of the sorption of Hg(II) ions onto chitosan. Chem Eng J 133(1–3):311–316

Sun X, Peng B, Ji Y, Chen J, Li D (2008) The solid–liquid extraction of yttrium from rare earths by solvent (ionic liquid) impreganated resin coupled with complexing method. Sep Purif Technol 63(1):61–68

Suquila FA, de Oliveira LL, Tarley CR (2018) Restricted access copper imprinted poly (allylthiourea): the role of hydroxyethyl methacrylate (HEMA) and bovine serum albumin (BSA) on the sorptive performance of imprinted polymer. Chem Eng J 350(15):714–728

Tavlarides L, Bae J, Lee C (1987) Solvent extraction, membranes, and ion exchange in hydrometallurgical dilute metals separation. Sep Sci Technol 22(2–3):581–617

Wei X, Xu G, Gong C, Qin F, Gong X, Li C (2018a) Fabrication and evaluation of sulfanilamide-imprinted composite sensors by developing a custom-tailored strategy. Sens Actuator B Chem 255:2697–2703

Wei X, Yu M, Li C, Gong X, Qin F, Wang Z (2018b) Magnetic nanoparticles coated with a molecularly imprinted polymer doped with manganese-doped ZnS quantum dots for the determination of 2, 4, 6-trichlorophenol. Microchim Acta 185(4):208

Wei X, Zhang Z, Wang Z (2019) A simple dopamine detection method based on fluorescence analysis and dopamine polymerization. Microchem J 145:55–58

Yu P, Wang H-Q, Bao R-Y, Liu Z, Yang W, Xie B-H, Yang M-B (2017) Self-assembled sponge-like chitosan/reduced graphene oxide/montmorillonite composite hydrogels without cross-linking of chitosan for effective Cr(VI) sorption. ACS Sustain Chem Eng 5(2):1557–1566

Zheng X, Liu E, Zhang F, Dai J, Yan Y, Li C (2016) Selective adsorption and separation of gadolinium with three-dimensionally interconnected macroporous imprinted chitosan films. Cellulose 24(2):977–988

Zheng X, Zhang Y, Zhang F, Li Z, Yan Y (2018) Dual-template docking oriented ionic imprinted bilayer mesoporous films with efficient recovery of neodymium and dysprosium. J Hazard Mater 353:496–504

Zheng X, Wang Y, Qiu F, Li Z, Yan Y (2019a) Dual-functional mesoporous films templated by cellulose nanocrystals for the selective adsorption of lithium and rubidium. J Chem Eng Data 64(3):926–933

Zheng X, Zhang Y, Bian T, Zhang Y, Zhang F, Yan Y (2019b) Selective extraction of gadolinium using free-standing imprinted mesoporous carboxymethyl chitosan films with high capacity. Cellulose 26(2):1209–1219

Zhu C, Hu T, Tang L, Zeng G, Deng Y, Lu Y, Fang S, Wang J, Liu Y, Yu J (2018) Highly efficient extraction of lead ions from smelting wastewater, slag and contaminated soil by two-dimensional montmorillonite-based surface ion imprinted polymer absorbent. Chemosphere 209:246–257

Publisher's Note Springer Nature remains neutral with regard to jurisdictional claims in published maps and institutional affiliations.